Exploring the harmful textile and pharmaceutical industries pollutant degradation mechanism and biological applications of MgO – SiO2 nanocomposite for environmental sustainability

Haewon Byeon[1], N. Shalom[2], Amaravadi Rama Krishna[3], Megala Rajendran[4], M. C. Priyadarshini[5], Anu Tonk[6] and J. Sunil[7]*

[1]College of AI Convergence, Inje University, Gimhae, Republic of Korea

[2]Department of Mechanical Engineering, Noorul Islam Centre for Higher Education, Kumaracoil, India

[3]Department of Physics, School of Basic and Applied Sciences, JSPM University, Pune, India

[4]Faculty of Humanities & Pedagogy, Turan International University, Namangan, Uzbekistan

[5]Vel Tech Rangarajan Dr.Sagunthala R&D Institute of Science and Technology, Chennai, Tamil Nadu, India

[67]Department of Multidisciplinary Engineering, The NorthCap University, Gurugram, Haryana, India
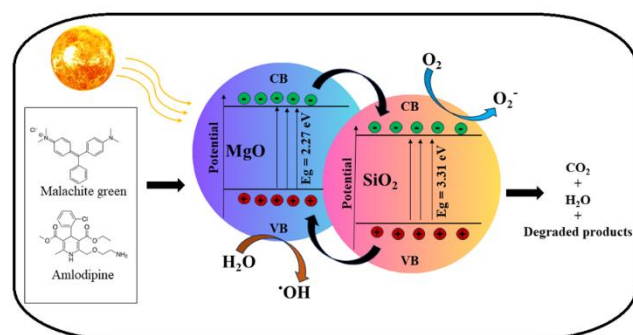
[7]Department of Mechanical Engineering, Annai Vailankanni College of Engineering, Kanyakumari, Tamil Nadu, India

Graphical abstract

Abstract

This article represents the photocatalytic activity of harmful pollutants from textile and pharmaceutical industries and compares the photocatalytic efficiency between pure MgO and MgO – SiO₂ nanocomposite. The MgO NPs are synthesized using hydrothermal synthesis, in which the extract from *Nerium oleander* flowers is utilized as a reducing agent. The SiO₂ NPs were synthesized from the natural source of bamboo leaves by sol-gel method. Then, the composite is made by simply stirring and sonicating MgO and SiO₂ NPs. Then the prepared nanocomposite and pure MgO were analyzed for the crystalline nature (XRD), morphology (FE-SEM), particle size (DLS), Functional groups (FTIR), elemental composition (EDAX), optical properties (UV-vis spectroscopy). The above studies provide excellent MgO NPs and MgO – SiO₂ composite characteristics. The prepared MgO and MgO - SiO₂ were utilized for the photocatalytic activity of textile and pharmaceutical pollutants up to 90 and 120 mins, respectively, under sunlight irradiation. After degradation, the photocatalysts were tested to find their stability and reusability for five cycles. As discussed above, the MgO – SiO₂ performs better than pure MgO in terms of pollutant degradation and stability. The prepared MgO and MgO – SiO₂ have been examined for antibacterial activity, exposing better results than the standard antibacterial agent (*Streptomycin*).

Keywords: Textile industries, pharmaceutical industries, Water pollution, Photocatalytic activity, antibacterial agent

1. Introduction

Water pollution has grown to be a significant worldwide problem that calls for the emergence of ideas for the execution and monitoring of plans that will eventually result in remedies. Discharging hazardous and toxic materials from various process industries has resulted in highly polluted environmental compartments (Sharma *et al.* 2021). The chemical and product manufacturing industries release toxic organic and inorganic compounds into neighbouring streams, including tanneries, oil refineries, petrochemical plants, textile mills, paper, dye and pigments, pharmaceuticals, and the cosmetics and oil industries. This pollution of aquatic environments results from these releases. Inadequate sanitation practices are a significant cause of water pollution and have contaminated water supplies globally. Over 2.5 billion people globally suffer from insufficient sanitation (Beard *et al.* 2022). In regions of the world, nearly one-third of amphibians and more than half of the native freshwater fish species are in danger of going extinct. An increase in the number of chemicals identified as posing environmental dangers to living things has resulted from the rapid development of resources and technology. The non-biodegradable nature, elevated chemical oxygen demand (COD), vivid colour, and strong odor of dyes used

in leather and textile industries, along with the large amounts of sludge generated during wastewater treatment, render these wastewaters highly harmful to the environment (Rathi *et al.* 2021). The pharmaceutical industry's explosive growth leads to the large-scale discharge of effluents containing many medication classes that harm the environment. Furthermore, it is essential to emphasize that many chemicals and other wastewater components are harmful and hardly biodegradable (Dhruv *et al.* 2022). These dangerous pollutants significantly affect the environment and lead to the demolition of wildlife and aquatic animals. Hence, the removal of these pollutants is a significant concern. Malachite Green is a toxic organic compound widely used as a dye, known for its harmful effects on human health and the atmosphere. Acute exposure may cause respiratory, skin, and gastrointestinal irritation, while chronic exposure is linked to carcinogenic, mutagenic, and organ toxicity effects (Sharma *et al.* 2023). Environmentally, it is highly toxic to aquatic life, leading to bioaccumulation and persistent contamination in water and soil. Amlodipine, primarily used to treat high blood pressure and angina, can have harmful environmental effects if it enters water systems as a pollutant. It is toxic to aquatic organisms, potentially disrupting reproductive and developmental processes and leading to bioaccumulation within the food chain.

Additionally, its presence in the environment can contribute to developing drug-resistant bacteria and pose health risks if trace amounts contaminate drinking water sources (Samreen *et al.* 2021). Hence, these harmful pollutants must be eliminated before they are put into water bodies. Photocatalytic activity in water treatment offers several benefits over conventional methods, including the effective degradation and complete mineralization of a wide range of organic pollutants and pathogens without producing harmful by-products (Al-Nuaim *et al.* 2023). It is energy-efficient, mainly when powered by sunlight, and does not require the addition of hazardous chemicals, reducing secondary pollution risks. The process allows for the regeneration and reuse of photocatalysts, enhancing sustainability, and can be easily integrated with other treatment methods for improved efficiency (Constantino *et al.* 2022). These advantages make photocatalysis a highly attractive, cost-effective, and environmentally friendly option for water purification. After oxygen, silica is the second element that is abundantly available on Earth. There are several methods for extracting the elements, which may be found in natural sources or synthesized from agricultural waste or crops. By use silica nanoparticles are a commonly utilized nanomaterial in many different technologies. Generally speaking, silica has a wide range of uses in manufacturing, adsorption processes, biosensing, packaging, and agriculture. Silica is a well-known composite material with metal oxides due to its enhanced surface area and adaptability.

Bamboo is an agricultural plant among the world's fastest-growing woody plants. Bamboo grows in various conditions, from freezing zones to near hot springs. According to estimates, between 30 and 50 million hectares of land on Earth are covered with various varieties of bamboo, most of which are farmed in Asian countries. After bagasse and rice husk, bamboo is the source of natural silica components, with the highest percentage (around 70%) in silica nanoparticles (SiO_2) production. According to their research, there is around 62.72% silica concentration in the ashes of bamboo leaves (Mohd *et al.* 2020). The *Nerium oleander* is a shrub that belongs to the *Apocynaceae* family and is evergreen (Demır *et al.* 2021). Every one of its components is poisonous. It treats dermatitis, emetics, scabies, ringworm, psoriasis, herpes, epilepsy, asthma, malaria, heart tonics, skin cancer, and tumors. Because of its distinctive features, magnesium oxide nanoparticles (MgO NPs) are one of the metal oxides used in industry, research, and medicine (Chinthala *et al.* 2021). A vital mineral, MgO NPs can destroy harmful compounds and have antibacterial and nutritious qualities. These NPs also have a high band gap and may be used as an electrical insulation addition in paints, superconductors, and refractory goods. This characteristic has shown the potential of MgO NPs as a helpful material in photocatalytic activity.

In this work, the SiO_2 has been synthesized from a natural source (Bamboo leaves) through the sol-gel process, and MgO NPs were produced through green synthesis using *Nerium oleander* flower extract. The prepared nanoparticles were made into a composite using ultrasonic waves. The prepared composite was characterized by its crystalline nature, structural phase, functional groups, morphology, particle size, and optical properties. The photocatalytic performance against Malachite green and amlodipine pollutants was done in sunlight, and its kinetics are revealed below.

2. Methodology

2.1. Materials

Chemicals used to prepare MgO NPs and SiO_2 were Magnesium nitrate, ethanol, HCl, NaOH, Bamboo leaves, and *Nerium oleander* flowers. Malachite green and Amlodipine were used as a model pollutant for photocatalytic degradation. The bacterial activity has been done using Streptococcus aureus and Escherichia coli. All the chemical reagents were purchased from Merck.

2.2. Preparation of raw materials

In an adjacent forest in Tamil Nadu, fresh bamboo leaves were gathered. To remove any undesirable particles, the leaves are cleaned in water and then in ionized water. After being cleaned, the leaves are dried at 105℃ and then calcined at 600℃ to yield ashes.

2.3. Synthesis of SiO_2 NPs

The sol-gel method was used to prepare the sample. Washing bamboo leaves is the initial stage in the preparation process, followed by calcination at 600℃. After immersing bamboo leaf ash (BLA) in HCl overnight and stirring it with a 1M NaOH solution for four hours, sodium silicate was extracted from the BLA. After that, the mixture was filtered with Whatman-No.1 filter paper to

remove any remaining carbon residue or particles, and the gel residue was obtained by washing it with distilled water. During the synthesis step, sodium silicate was produced. 3M HCl was used to acidify the solution's pH until it became neutral. The mixture ages for eighteen hours before being dried at 60℃ for four hours, yielding SiO_2 NPs.

2.4. Preparation of Nerium oleander flower extract

The Flowers of *Nerium oleander* are collected from the plant, then washed and dried in the shade to avoid the loss of phytochemicals. After that, a mixer grinder set to 10000 rpm was used to grind the dried leaves into a powder. To make an extract, 5g of the obtained powder was mixed in 100 mL of hot DD water and stirred at 60°C for an hour and without heat for 24 hours for the maximum extraction of phytochemicals from the leaf extract. The phytochemicals show a significant role in nanoparticle formation, which reduces and caps over the surface of the MgO NPs. After stirring, the solution was filtered using a Whatman filter paper for further use.

2.5. Synthesis of MgO NPs

About 100 mL of the prepared leaves extract is taken in a beaker, and magnesium nitrate is added according to its stoichiometry ratio and mixed thoroughly. Then, the solution was transferred to a teflon container for the hydrothermal setup. The hydrothermal setup was kept in a hot air oven at 80℃ for 12 hours. Then, to remove contaminants, they are cleaned and dried for three hours at 60℃ in a hot air oven. After that, the powder is calcined for three hours at 400℃ to remove any volatile contaminants and create a crystalline structure (**Figure 1**).
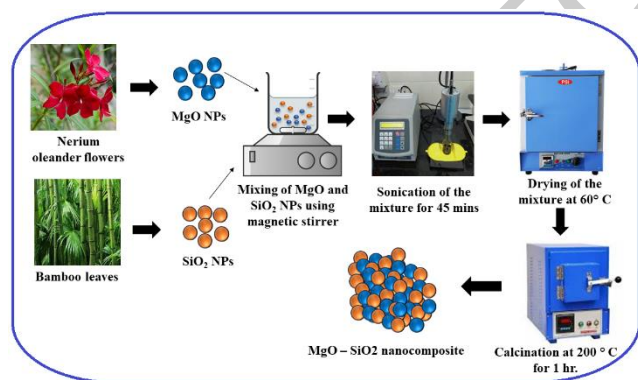

Figure 1. Preparation of MgO – SiO₂ nanocomposite through sonication method

2.6. Preparation of MgO – SiO₂ composite

The prepared MgO and SiO_2 NPs were taken in an equal weight ratio (1:1) and mixed thoroughly under distilled water using a magnetic stirrer. Then, the mixed solution was sonicated for up to 45 minutes to ensure the uniform distribution of nanoparticles. Afterward, they were dried at 60℃ over 6 hours and calcined at 200℃ over 1 hour to bind dissimilar nanoparticles. After calcination, the nanocomposite is collected and stored for further use.

2.7. Sample preparation for photocatalytic degradation

The photocatalytic degradation of malachite green and Amlodipine in the presence of MgO and MgO – SiO₂

nanocomposite under sunlight was analysed as follows. Both malachite green and amlodipine pollutants of 100 mg were mixed thoroughly in 100 mL of deionized water and stored as a stock solution. Then, 100 mg of the prepared MgO and MgO – SiO₂ nanocomposite were added separately to the pollutants. The nanoparticle-suspended pollutants were irradiated under sunlight for over 90 and 120 minutes for Malachite green and Amlodipine, respectively. A UV-vis spectroscopy examination was performed on the appropriate quantity of pollutants at intervals of 15 minutes. After that, the deterioration was assessed based on their degree of optical absorption, and the UV-vis spectrum was recorded regularly. Further, the efficiency of the pollutant degradation of the nanomaterials was revealed using the equation (1) below.

$$\text{Degradation efficiency} \left(\%\right) = \left(1 - \frac{Ct}{C0}\right) \times 100 \qquad (1)$$

Where c_t and c_0 are the final and initial concentrations of the respective pollutants.

2.8. Preparation of MHA medium

Mueller-Hinton agar medium is made by measuring one liter of distilled water, adding 38 grams of Mueller-Hinton agar powder, and stirring to prevent clumping. Stir and warm gradually until completely dissolved. Autoclave at 121°C for 15 minutes to sterilise. Once 45–50°C has cooled, transfer the mixture onto sterile Petri dishes, filling each to a depth of about 4 mm (25–30 mL). Allow the agar to firm at room temperature, then store the plates in a covered container at 4°C until needed. Don't forget to mark the plates with the preparation date and media type. To avoid contamination, sterile procedures should be kept up at all times. Then, the agar medium was swabbed with bacteria using sterile earbuds, and holes were made using a micropipette needle. The holes were filled with different concentrations of the NPs, such as 25, 50, and 100 mg/mL, and streptomycin was used as a standard. Then the inhibited zone was measured after an incubation period of 24 hours using a screw gauge.

2.9. Characterization methods

The structural properties of the synthesized MgO NPs were examined by a powder X-ray diffractometer (PANalytical, Almelo, the Netherlands). The FTIR spectroscopy (PerkinElmer, USA) was used for MgO and MgO – SiO₂ in the 400–4000 cm^{-1} range to record the molecular vibration and functional groups. An identical pellet was created when KBr and a powder sample were mixed in a 200:1 ratio. The KBr functioned as the IR source's active medium. A 633 nm laser light source and the dynamic light scattering concept, particle size distribution (Nanophox;), were used to calculate the average particle size distribution. The EDX and FESEM were used to examine the surface texture and morphology of MgO NPS to determine the material's elemental composition. The level of the optical absorbance of synthesized MgO NPs and MgO – SiO₂ was evaluated using a UV-Vis spectrophotometer (Cary 8454, Singapore).

3. Results and discussions

3.1. X-ray diffraction analysis

Using XRD analysis, the produced MgO and MgO – SiO$_2$ composite's crystal structure, structural phase, and size of the crystals were identified (**Figure 2**). The emerged peak positions of MgO NPs are 37.28, 42.39, 62.75, 74.86, and 78.78, which correspond to the plane of (002), (101), (103), (004), and (202), respectively. The MgO powder's 2θ locations correspond with JCPDS card no. 75-0447 (Zhu *et al.* 2020), indicating that the produced MgO NPs are very pure and crystalline and lack additional diffraction peaks. The MgO NPs are identified as cubic structures with a calculated crystal size of 23 nm. The MgO NPs show a high crystalline nature due to the phytochemicals present in the flowers of *Nerium oleander* (Chandrasekaran *et al.* 2024). Meanwhile, in the MgO – SiO$_2$ nanocomposite, the SiO$_2$ diffraction peak dominates the MgO peak because the atomic radius of SiO$_2$ is slightly higher than that of MgO. The identified peak position at 19.86 indicates the formation of SiO$_2$, which corresponds to the Miller indices (001). It is noted that the MgO peak at 40.67 shifted from 42.39, indicating the effective formation of the composite. The observed 2θ position of SiO$_2$ agrees with the JCPDS NO: 85 – 0335 (Wang *et al.* 2023), indicating that the prepared SiO$_2$ is crystalline, pure, and hexagonal structure. The crystal structure of the prepared MgO – SiO$_2$ nanocomposite is found to be 30.72 nm.
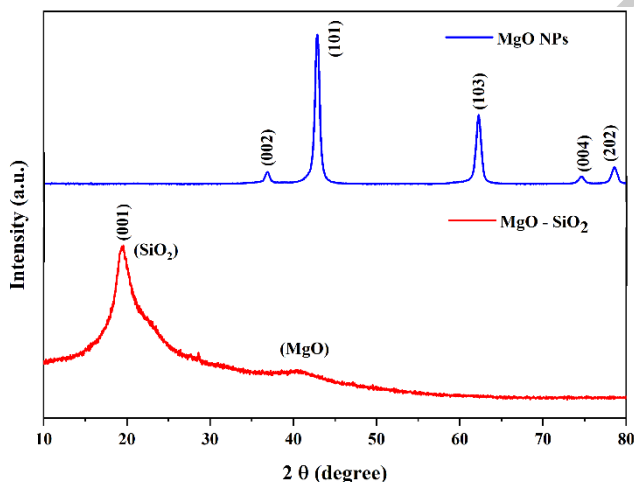

Figure 2. XRD analysis of MgO and MgO– SiO$_2$ nanocomposite

3.2. Morphology analysis

The surface topography of the prepared MgO and MgO – SiO$_2$ nanocomposites has been determined using FESEM, depicted in **Figure 3 (a and b)**. From the figures, it is identified that the prepared MgO NPs own a monodispersed spherical morphology. This indicates the excellent properties of phytochemicals in the *Nerium oleander* flower extract, which could effectively reduce chloride precursors and convert metal oxide through a chemical reduction process (Jeevanandam *et al.* 2022). Similarly, the morphology of the composite is noted as agglomerated spheres. It indicated that adding SiO$_2$ with MgO induces the particles' surface charge, which may be due to the presence of phytochemical compounds at the surface of the composite (Naren *et al.* 2024). The particle

sizes of MgO and MgO – SiO$_2$ composites are at a nano range that fits the previous XRD and PSA findings. The EDAX mapping is analyzed to find the overall elemental composition of the prepared MgO – SiO$_2$ composite, as seen in **Figure 3(c)**. The analysis shows the K shell's composition occurrence of Mg, O, and Si. The absence of other elements represents the high purity of pure MgO and MgO – SiO$_2$ composite. The presence of MgO is higher than SiO$_2$, which fits the XRD results. Elemental mapping has been taken to analyze the presence of various elements in a specific area (Zhang *et al.* 2021). It shows the presence and position of Mg, Si, and O elements in the overlay image, confirming the high purity of the composite shown in **Figure 4**.
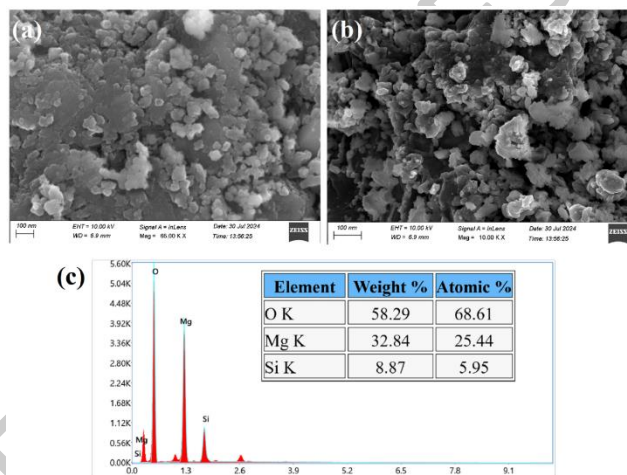

Figure 3. Morphological (a & b) and elemental analysis (c) of MgO and MgO – SiO$_2$ nanocomposite
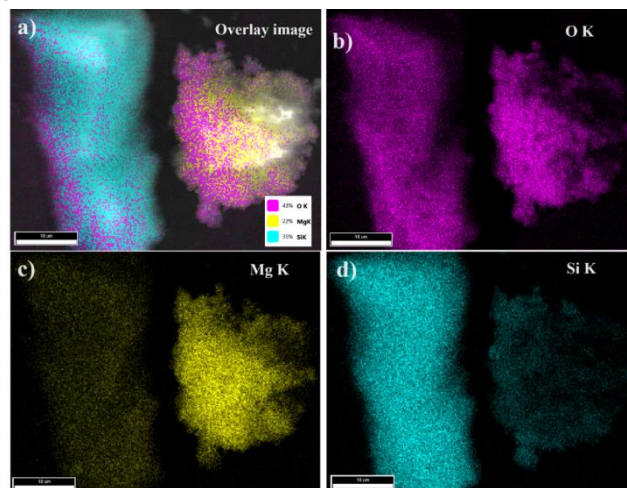

Figure 4. Elemental mapping for the prepared MgO – SiO$_2$ nanocomposite

3.3. FTIR Results

The presence of multiple functional groups in the prepared MgO NPs and MgO – SiO$_2$ nanocomposite was determined using FTIR, as shown in **Figure 5**. The most common peaks in MgO and MgO – SiO$_2$ composites emerge at 3430, 2924, 2851, 1639, 1416, and 567 cm^{-1}. Stretching of the hydrogen and alcohol groups is the cause of the prominent FTIR band at 3428 cm^{-1} (Devabharathi *et al.* 2024). The emergence of symmetrical and asymmetrical vibration of the =CH$_2$ and -CH$_3$ groups, which suggests the alkanes' availability, is responsible for

the mild peak at 2932 cm^{-1} and 2849 cm^{-1}. Aromatic amines with an N-H vibrational mode are responsible for the peak at 1642 cm^{-1} (Jagan *et al.* 2023). Mild carboxyl stretching at 1103 cm^{-1}, which functions as a reducing agent at the moment of production of nanoparticles in the green synthesis process, indicates the existence of alcohols and phenols. Further, a bond between Mg and O is revealed by a transmission peak at 567 cm^{-1}. Further, the intense peak is additionally seen in the MgO – SiO$_2$ composite at 1085 cm^{-1}, confirming the availability of Si-O formation (Karan *et al.* 2021). Both MgO and SiO$_2$ peaks are found in the composite, which indicates that the composite formation is without additional impurities.
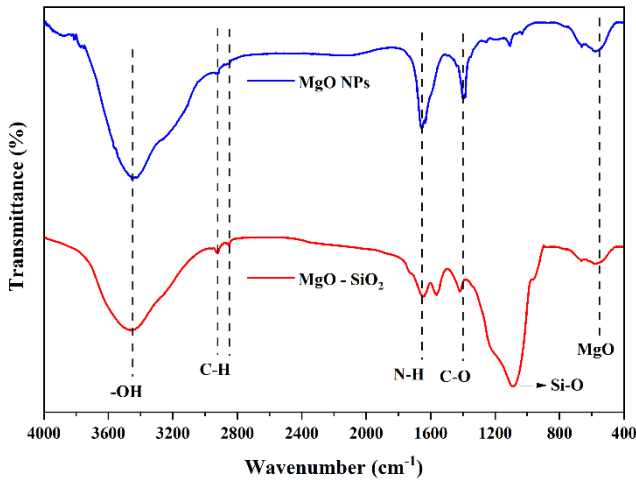

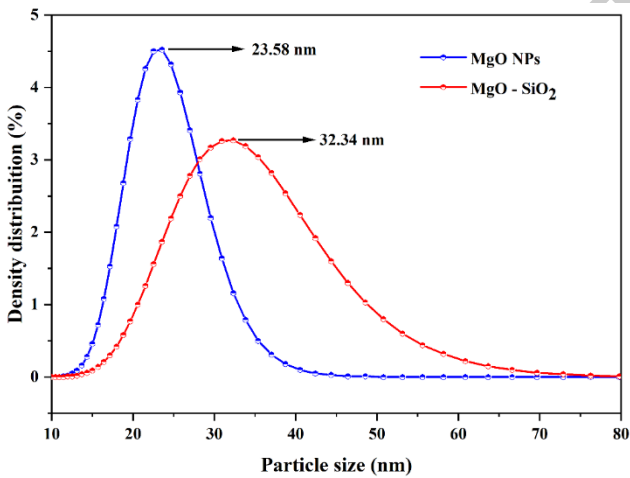**Figure 5.** FTIR analysis for MgO and MgO – SiO$_2$ nanocomposite

Figure 6. DLS analysis for MgO and MgO – SiO$_2$ nanocomposite

3.4. Dynamic light scattering

The mean size of the prepared MgO and MgO – SiO$_2$ nanocomposite were analyzed through a dynamic light scattering technique in which the Brownian motion is utilized to measure the mean particle size, as seen in **Figure 6**. The average particle size (d_{50}) of MgO and MgO – SiO$_2$ are 23.58 and 32.34 nm, respectively. The particle size increases due to the addition of SiO$_2$ with MgO NPs. The d_{10} (minimum) and d_{90} (maximum) particle sizes of MgO are 11.56 and 40.63 nm, respectively. Similarly, the d_{10} and d_{90} for the composite are 15.32 and 63.52 nm, respectively. The results suggest that the prepared MgO and MgO – SiO$_2$ nanocomposites are ultrafine nanoparticles. The broad peak in the composite indicates

that the maximum size of the particles occurs in the d_{50} (32.34 nm) range (Jagan *et al.* 2023).

3.5. UV – Visible spectroscopy

Figure 7 displays the UV-vis spectra of pure MgO and MgO – SiO$_2$. MgO nanoparticles spectra show one distinct band at 211 nm and MgO- SiO$_2$ at 225 and 269 nm (Nahrawy *et al.* 2020). It is noted that MgO is red-shifted after adding SiO$_2$, indicating the composite's successful formation. The optical-electronic transition of MgO and SiO$_2$ is represented by the peak in the UV region, which has been noticed.
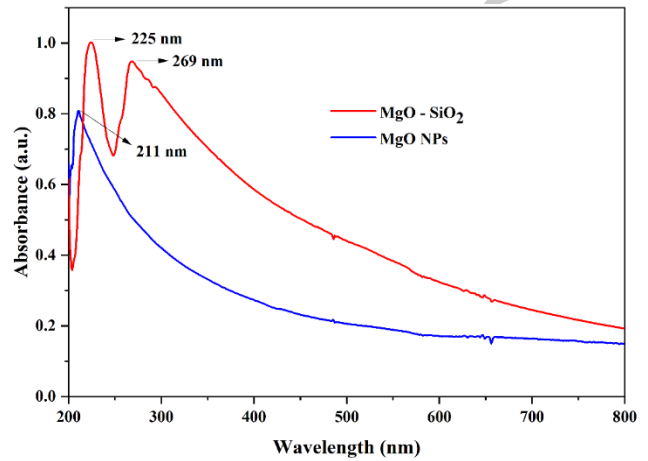

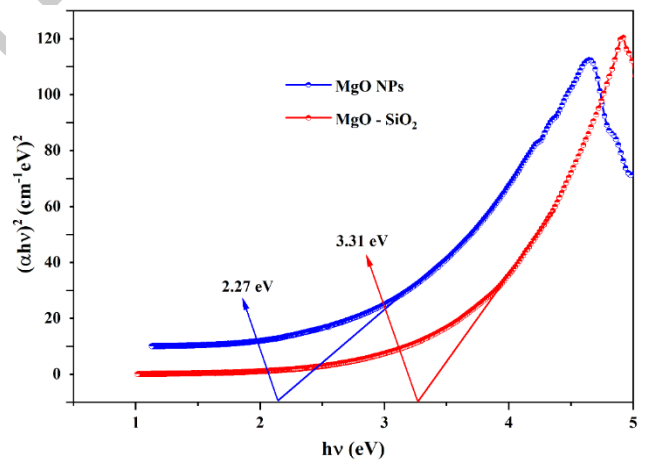**Figure 7.** UV-vis spectrum of the MgO and MgO – SiO$_2$ nanocomposite

Figure 8. Calculated bandgap for the MgO and MgO – SiO$_2$ nanocomposite

Tauc's plot established the direct bandgap for MgO and MgO – SiO$_2$ NPs from the obtained absorption spectra. Using the formula (Equation 2), the absorption efficiency and incident photon energy are correlated (Nahrawy *et al.* 2020),

$$\alpha(\upsilon)h = K\left(h\upsilon - Eg\right)^{n} \qquad (3)$$

The calculated band gap of the prepared MgO and MgO – SiO$_2$ is 2.27 and 3.31 eV, respectively, shown in **Figure 8**. The band gap is the area with the slightest energy difference between the valence band's top and the conduction band's bottom. The silicon addition is responsible for the composite's more significant band gap,

which might boost photocatalytic efficiency by increasing the recombination rate.

3.6. Electrochemical impedance spectroscopy

Figure 9 shows a Nyquist plot of the MgO- SiO₂ nanocomposite at the open-circuit potential state compared to that of MgO in 1 M KOH under light irradiation. The semicircle of MgO – SiO₂ decreases from pure MgO, leading to a decrease in charge transfer resistance that enables free charge flow. As a recombination suppression mechanism, reduced charge transfer resistance enhanced the charge transport to the electrolyte. The creation of Si+ surface states, which function as intermediaries for charge transfer to the electrolyte, may be the reason for the MgO – SiO₂ system's superior performance compared to pure MgO (Jiao *et al.* 2020). The impedance measurement findings showed that the suitable equivalent circuits were fitted for all analyses. In the electrolyte, the MgO – SiO₂ electrodes showed a lower charge transfer resistance than the MgO electrodes. Because SiO₂ is added to the MgO band gap, the charge transfer resistance of MgO - SiO₂ is greater than that of pure MgO. This behavior in the MgO – SiO₂ system is because SiO₂ stores energy when exposed to photon deprivation. Because the electron's charge transfer to the semiconductor surface occurs more quickly, more electrons are available to form radicals that react with the contaminants (Ramalingam *et al.* 2022). Next, it was established that photogenerated carriers recombine slowly.
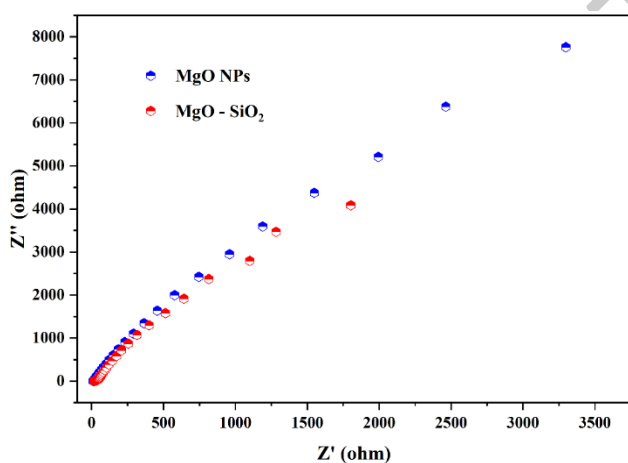
Figure 9. EIS analysis for MgO and MgO – SiO₂ nanocomposite

3.7. Photocatalytic activity

The photocatalytic degradation of textile (Malachite green) and pharmaceutical pollutants (Amlodipine) in the presence of prepared MgO and MgO – SiO₂ under sunlight irradiation is depicted in **Figures 10 and 11**. The optical absorption has been analyzed under various conditions, such as without light or catalyst. Without light, the MgO – SiO₂ nano photocatalyst was mixed with the pollutants and analyzed in the dark.

The degradation of pollutants was determined by the intensity of the decay of the characteristic peaks around 368 (Amlodipine) and 528 nm (Malachite green) as a function of irradiation time (t). The pollutants' absorption decreases gradually, indicating that the nanocatalyst

performs a catalytic reaction that breaks down its molecules effectively (Bisaria *et al.* 2021). The calculated degradation efficiency of MgO and MgO – SiO₂ against malachite green is 81.56 and 98.67 %, respectively, within 90 mins. Similarly, for Amlodipine, the degradation efficiency is 76.27% and 97.26 % for MgO and MgO – SiO₂ nanocomposite, respectively, over 120 mins. The time taken to degrade pharmaceutical pollutants is slightly higher than that of textile pollutants under sunlight. This may be due to the compact structure of Amlodipine, which makes it difficult for the photocatalyst to deform the structure of the pollutant. The degradation efficiency of malachite green and Amlodipine without a catalyst is 1.3 and 1.5 %, respectively, and in the case without light and presence of MgO – SiO₂ photocatalyst, is 9.7 and 6.32 %, respectively, which intimates the importance of both sunlight and photocatalyst in the degradation process.
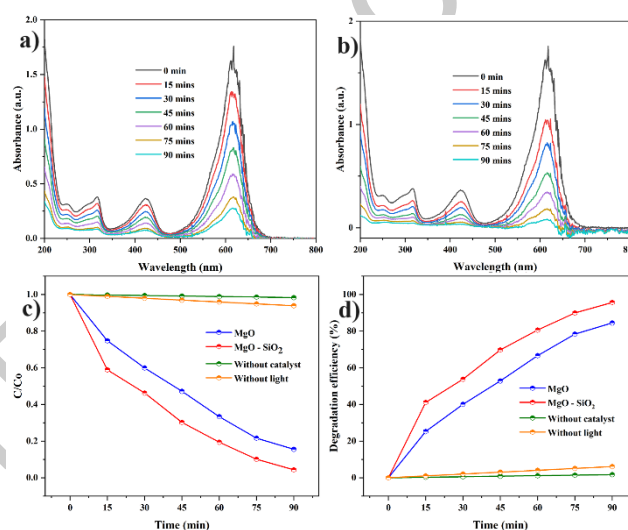
Figure 10. Photocatalytic performance on Malachite green a) MgO, b) MgO – SiO₂, c) C/Co, and d) degradation efficiency
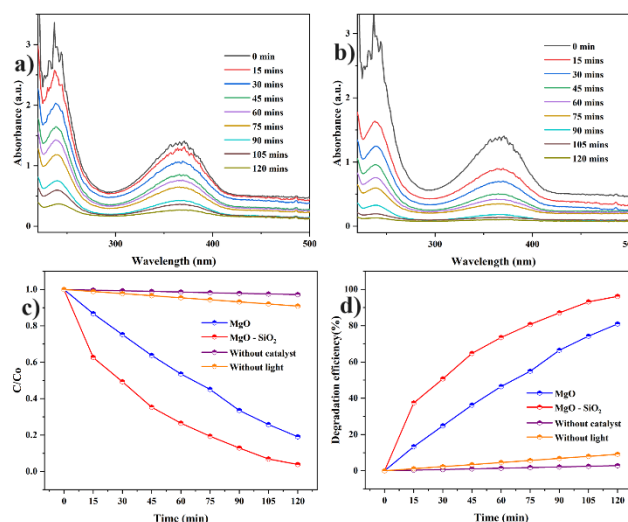
Figure 11. Photocatalytic degradation on Amlodipine a) MgO, b) MgO – SiO₂, c) C/Co, and d) degradation efficiency

As seen in Figure 12, the photocatalytic degradation of produced nanocatalysts against malachite green and Amlodipine follows pseudo-first-order kinetic processes. The equation (3) examines the pseudo-first-order kinetics (Nemiwal *et al.* 2021).
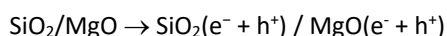
$$Ln\frac{C}{Co} = kt \tag{3}$$

Where, C is the absorption of pollutants at different periods, and C_o represents the initial concentration of dye. K and t indicate the degradation constant and time of reaction, respectively. The degradation rate of MgO, MgO – SiO$_2$, without catalyst, and without light against malachite green is 0.206, 0.328, 0.0002, and 0.0007 min^{-1} respectively. Similarly, the degradation rate for Amlodipine is 0.135, 0.0255, 0.0002, and 0.0008 min^{-1} for MgO, MgO – SiO$_2$, without catalyst, and light, respectively. The degradation rate is higher for the composite than pure MgO due to the addition of SiO$_2$ NPs that increases the bandgap of the material, improving the recombination rate and showing degradation efficiency (Nemiwal *et al.*

2021). The Comparison of the photocatalytic activity of various composites of SiO$_2$ and MgO over various pollutants is depicted in **Table 1**.
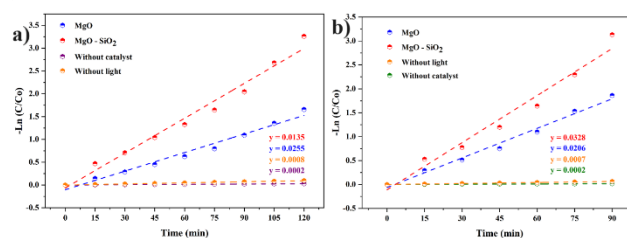

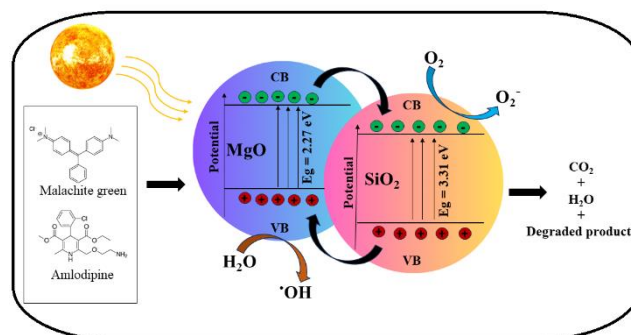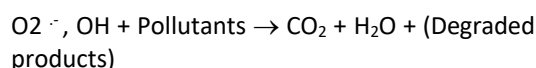**Figure 12.** Pseudo–first-order degradation kinetics of Amlodipine (a) and Malachite green (b)

Table 1. Comparison of the photocatalytic activity of various composites of SiO$_2$ and MgO over various pollutants

Composite	Pollutant	Time (min)	Efficiency (%)	Ref
SiO$_2$ - MgO	Tetracycline	90	85.8 %	37
SiO$_2$ – Fe$_2$O$_3$	Rhodamine B	150	75 %	38
SiO$_2$ – TiO2	Methylene blue	90	96.1 %	39
Mg- SiO$_2$-Zn	Chromium	120	72.75 %	40
MgO – SiO$_2$	Lead	60	60 %	41
MgO – SnO$_2$	Sunset Yellow	60	99 %	42
SiO$_2$ – gC$_3$N$_4$	Xenyl orange	120	84.6 %	43
TiO$_2$ – SiO$_2$ - MWCNT	acetaminophen	60	81.6 %	44
MgO	Malachite green	90	81.56 %	
MgO – SiO$_2$			98.67 %	
MgO	Amlodipine	120	76.27 %	
MgO – SiO$_2$			97.26 %	

4. Dye degradation mechanism

The four processes of light exposure, photoexcitation, separation, and electron and hole transport to the catalyst surface, where they respond to the pollutants via an oxidation-reduction reaction, are necessary to break down the dangerous pollutants via photocatalysis. The valence band (VB) electrons in MgO are stimulated to the conduction band (CB) upon exposure to light radiation, as seen in Figure 13. In the CB, polarised holes (h$^+$) are produced, whereas in the valence band (VB), electrons (e$^-$) are made. When electrons and holes come into contact with organic contaminants on the catalyst's surface, they undergo an oxidation-reduction process. Superoxide anions (O$_2^{\cdot-}$) are produced when oxygen, an electron acceptor, undergoes a reduction process with photogenerated electrons. Consequently, more organic pollutants are oxidized by superoxide anions, which may react with hydrogen ions to create hydrogen peroxide (H$_2$O$_2$). Furthermore, hydroxyl radical ($\cdot$OH) is produced when hydrogen peroxide combines with superoxide anions. Organic material (pollutants), superoxide anions (O$_2^{\cdot-}$), and hydroxyl radicals ($\cdot$OH) may mineralize on the catalyst's surface to produce degradation products, including carbon dioxide (CO$_2$) and H$_2$O ions (Naggar *et al.* 2023).

$$SiO_2/MgO \rightarrow SiO_2(e^- + h^+) / MgO(e^- + h^+)$$

$$SiO2 (e^- + h^+) / MgO (e^- + h^+) \rightarrow SiO_2 (e^-) / MgO (h^+)$$

$$e^- + O2 \rightarrow O2.^-$$

$$e^- + H^+ + O2^{\cdot-} \rightarrow H_2O_2$$

$$H_2O_2 + O^{\cdot-} \rightarrow OH + OH^-$$

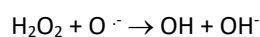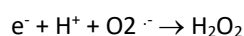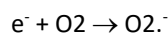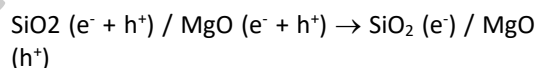$$O2^{\cdot-}, OH + Pollutants \rightarrow CO_2 + H_2O + (Degraded products)$$

Figure 13. Pollutant degradation mechanism for MgO – SiO$_2$ nanocomposite

4.1. Stability and reusability

For nanocatalyst to be used practically in large-scale industrial applications, they must be reusable. The method used to eliminate contaminants and other

unwanted molecules from wastewater systems considers several factors, including cost, efficiency, and reusability. Catalyst recycling and adsorbate regeneration are efficient processes. After photodegradation, the nanocatalyst was carefully cleaned using distilled hot water and dried in an oven for 180 minutes at 100 °C. The degradation efficiency was assessed by monitoring the decrease in absorption of pollutants over irradiation time, as depicted in **Figure 14**. Notably, a consistent reduction in degradation efficiency was detected after the 5th cycle for MgO and MgO – SiO$_2$ in the case of Malachite green dye, with losses of approximately 7.2 and 4.8 %, respectively. Similarly, for Amlodipine, the degradation efficiency exhibited losses of around 8.3 and 4.1 % for MgO and MgO – SiO$_2$ composite, respectively. The decline in cyclic stability may be determined by the surface adsorption of pollutants, which decreases the active sites on the photocatalyst's surface, hindering photon and pollutant interactions. Despite these minor losses, the overall cyclic stability of the nanoparticles remains, affirming the suitability of the prepared MgO – SiO$_2$ nanocomposite as stable nano photocatalysts for pollutant degradation (Abuelgasim *et al.* 2023). The addition of SiO$_2$ in MgO gives improved stability compared to pure MgO, in which SiO$_2$ prevents the loss of active sites and provides stability for MgO NPs.
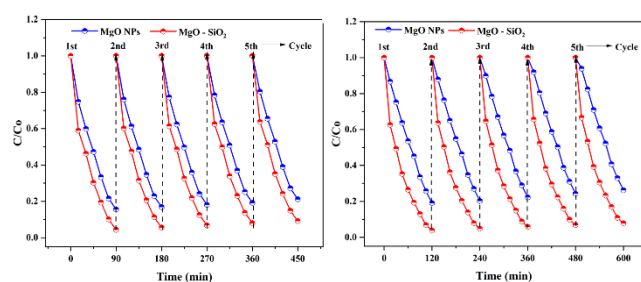

Figure 14. Stability and reusability of MgO and MgO – SiO$_2$ over malachite green (a) and Amlodipine (b)

4.2. Antibacterial activity

The prepared MgO and MgO – SiO$_2$ nanocomposite displayed antibacterial activity towards the tested gram-positive bacterial strain of *S. aureus* and gram-negative strain *E. coli,* as shown in **Figure 15** and measured in **Table 2**. *S. aureus* exhibits the highest sensitivity to MgO – SiO$_2$ nanocomposite compared to the other strains. The disc diffusion test revealed that the composite negatively impacted the inhibitory zones. These nanoparticles may have intrinsic antibacterial properties as they may harm bacterial cell membranes and obstruct their metabolic processes. The figure indicates that both pure MgO and MgO – SiO$_2$ composites exhibit excellent antibacterial activity.

Table 2. Antibacterial activity of MgO and MgO – SiO$_2$ nanocomposite against E. coli and S. aureus bacteria

Sample	Inhibition zone (mm) – Concentrations (mg/mL)							
	S. aureus				*E. coli*			
	25	50	100	std	25	50	100	std
MgO	12	15	17	10	10	14	19	12
MgO – SiO$_2$	14	16	18	10	11	16	21	12

However, since SiO$_2$ NPs have a more extensive surface area than other materials and may establish good contact with bacteria, enhancing the antibacterial response, the MgO – SiO$_2$ composite displays somewhat better zone inhibition than pure MgO (Natrayan *et al.* 2024). The connection between the antibacterial efficiency and nano-silica incorporation is a crucial aspect of the composite design. Higher nano-silica levels are often associated with more effective antibacterial agents, which boost antimicrobial action. The improved antibacterial activity may also be attributed to the release of reactive oxygen species (ROS) in the nanocomposite due to the high recombination rate. As discussed above, this MgO – SiO2 releases more ROS than pure MgO. These ROS enter the cell wall of the bacteria and cause damage to interior organs that leads to cell death (Gao *et al.* 2021).
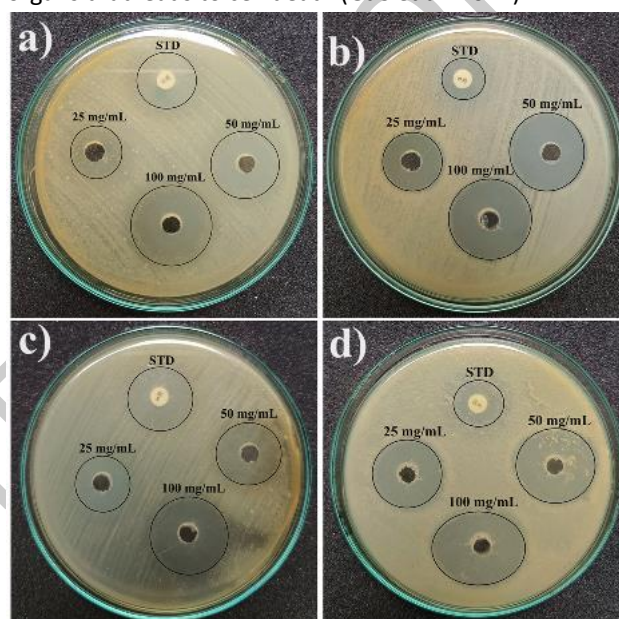

Figure 15. Antibacterial activity of MgO (a, b) and MgO – SiO$_2$ (c, d) composite against *E. coli* (a, c) and *S. aureus* (b, d)

5. Conclusion

The MgO has been successfully synthesized through the green synthesis method using *Nerium oleander* flower extract as a reducing agent. The SiO$_2$ was produced from the natural source of bamboo leaves by the sol-gel process. Then, the prepared MgO and SiO$_2$ were made into a composite using the hydrothermal method and characterized for their physio-chemical properties. The XRD results show the cubic structural phase with a mean crystal size of 30.72 nm. The FESEM reveals the spherical and agglomerated spherical morphology for MgO and MgO - SiO$_2$ nanocomposite, respectively. The FTIR results represent the occurrence of various functional groups and the existence of MgO – SiO$_2$ nanocomposite. The XRD, EDAX, and FTIR results confirm the formation of the MgO – SiO$_2$ composite without any other impurities, showing the nanocomposite's high purity. The calculated bandgap from the UV – vis spectroscopy is about 2.27 and 3.31 eV for MgO and MgO – SiO$_2,$ respectively. The increased bandgap may result in a higher electron recombination rate and efficient photocatalytic performance. The photocatalytic performance of malachite green against

MgO and MgO – SiO_2 is 81.56 and 98.67 %, respectively, within 90 mins.

Similarly, for Amlodipine, the degradation efficiency is 76.27% and 97.26 % for MgO and MgO – SiO_2 nanocomposite, respectively, over 120 mins. The process has been repeated five times to find the stability and reusability of the photocatalysts. The results indicate that MgO – SiO_2 shows enhanced stability in both pollutants due to the addition of SiO_2 in MgO NPs. The SiO_2 prevents the loss of active sites in the MgO NPs, reducing the photocatalysts' cost efficiency. The antibacterial activity has been examined for the prepared MgO and MgO – SiO_2 composite against *E. coli* and *S. aureus*, showing the maximum inhibition zone of 17 and 18 for *S. aureus* and 19 and 21 for *E. coli*. The article reveals that the prepared MgO – SiO_2 nanocomposite is a potential candidate for water treatment.

Acknowledgement

References

Abuelgasim S., Wang W. and Li T. (2023). Optimizing oxygen uncoupling performance and stability of novel MgO/TiO_2 supported CuO oxygen carrier: Effect of impregnation steps and ZrO_2 addition, *Separation and Purification Technology,* **326**, 124827.

Al-Nuaim M.A., Alwasiti A.A. and Shnain Z.Y. (2023). The photocatalytic process in the treatment of polluted water, *Chemical Papers*, **77**, 677–701.

Beard V.A., Satterthwaite D., Mitlin D. and Du J. (2022). Out of sight, out of mind: Understanding the sanitation crisis in global South cities, *Journal of Environmental Management,* **306,** 114285.

Bisaria K., Sinha S., Singh R. and Iqbal H.M.N. (2021). Recent advances in structural modifications of photocatalysts for organic pollutants degradation - A comprehensive review, *Chemosphere*, **284,** 131263.

Chandrasekaran N., Periakaruppan R. and Selvaraj K.S.V. (2024). Flower extract of Tagetes erecta (marigold) as capping agents for the synthesis of magnesium oxide nanoparticles with antioxidant potential, *Biomass Conversion and Biorefinery*, **24**, 05668.

Chinthala M., Balakrishnan A. and Venkataraman P. (2021). Synthesis and applications of nano-MgO and composites for medicine, energy, and environmental remediation: a review, *Environmental Chemistry Letters,***19**, 4415–4454.

Constantino D.S.M., Dias M.M. and Silva A.M.T. (2022). Intensification strategies for improving the performance of photocatalytic processes: A review, *Journal of Cleaner Production,* **340**, 130800.

Demir N. and Dasdemır S.N. (2021). Determination of industrially significant bioactive in oleander (Nerium oleander L) flowers with different Colors Utilized as Traditional Medicine, *International Journal of Innovative Research and Reviews*, **5**, 51–57

Devabharathi V., Jagan K.S.G. and Priyan S.R. (2024). Rational design of NiO nanoflakes and porous GCN nanocomposite for synergic effectiveness on photocatalytic degradation of industry effluents and biological activity, *Chemical Physics Impact*, **8**, 100637.

Dhruv D. and Bhatt S. (2022). Environmental pollution, toxicity profile, and physico-chemical and biotechnological approaches for treatment of textile wastewater, *Biotechnology and Genetic Engineering Reviews,* **3**, :33–86.

Jagan K.S.G., Surendhiran S. and Savitha S. (2023). Influence of different alkaline actuators in the synthesis of NiO NPs: A comparative green approach on photocatalytic and in vitro biological activity, *Inorganic Chemistry Communications,* **151**, 110618.

Jeevanandam J., Kiew S.F. and Boakye-Ansah S. (2022). Green approaches for the synthesis of metal and metal oxide nanoparticles using microbial and plant extracts, *Nanoscale,* **14,** 2534–2571.

Jiao S., Sun Z. and Wen J. (2020). Development of Rapid Curing SiO2 Aerogel Composite-Based Quasi-Solid-State Dye-Sensitized Solar Cells through Screen-Printing Technology, *ACS Appl Mater Interfaces,* **12**, 48794–48803.

Karan R., Pal P., Maiti P.K. and Das K. (2021). Structure, properties and in-vitro response of SiO_2-Na_2O-CaO-P_2O_5 system based glass-ceramics after partial replacement of Na_2O by Li_2O, *Journal of Non-Crystalline Solids,* **556**, 120554.

Mohd M.K.H. and Sapawe N. (2020). Removal of methyl orange over low-cost silica nanoparticles extracted from bamboo leaves ash, *Materials Today: Proceedings,* **31**, A54–A57.

Naggar A.H., Seaf-Elnasr T.A. and Thabet M. (2023). A hybrid mesoporous composite of SnO_2 and MgO for adsorption and photocatalytic degradation of anionic dye from real industrial effluent water, *Environmental Science and Pollution Research*, **30,** 108247–108262.

Nahrawy A.M., Elzwawy A., Abou A.B. and Mansour A.M. (2020). Influence of NiO on structural, optical, and magnetic properties of Al_2O_3–P_2O_5–Na_2O magnetic porous nanocomposites nucleated by SiO_2, *Solid State Sciences,* **108**, 106454.

Naren T.M., Surendhiran S. and Jagan K.S.G. (2024). Surface chemistry of phytochemical enriched MgO nanoparticles for antibacterial, antioxidant, and textile dye degradation applications, *Journal of Photochemistry and Photobiology A: Chemistry,* **448**, 115349.

Natrayan L., Ameen F. and Chinta N.D. (2024). Antibacterial and dynamical behavior of silicon nanoparticles influenced sustainable waste flax fiber-reinforced epoxy composite for biomedical application, *Green Processing and Synthesis,* 1**3,** 20230214.

Nemiwal M., Zhang T.C. and Kumar D. (2021). Recent progress in g-C3N4, TiO_2, and ZnO based photocatalysts for dye degradation: Strategies to improve photocatalytic activity, *Science of The Total Environment,* **767**, 144896.

Ramalingam G., Perumal N., Priya A.K. and Rajendran S. (2022). A review of graphene-based semiconductors for photocatalytic degradation of pollutants in wastewater, *Chemosphere,* **300**, 134391.

Rathi B.S. and Kumar P.S. (2021). Critical review on hazardous pollutants in the water environment: Occurrence, monitoring, fate, removal technologies, and risk assessment, *Science of The Total Environment,* **797**, 149134.

Samreen K., Ahmad I., Malak H.A. and Abulreesh H.H. (2021). Environmental antimicrobial resistance and its drivers: a potential threat to public health, *Journal of Global Antimicrobial Resistance,* **27**, 101–111.

Sharma J., Sharma S. and Soni V. (2023). Toxicity of malachite green on plants and its phytoremediation: A review, *Regional Studies in Marine Science,* **62**, 102911.

Sharma P. and Singh S.P. (2021). Pollutants characterization and toxicity assessment of pulp and paper industry sludge for safe environmental disposal. In: Haq I, Kalamdhad AS (eds), *Emerging Treatment Technologies for Waste Management*, **1**, 207–223.

Wang M., Jiao Y., Li N. and Su Y. (2023). Synthesis of a SiO$_2$-MgO composite material derived from yellow phosphorus slag with excellent malachite green adsorption activity, *Journal of Alloys and Compounds,* **969**, 172344.

Zhang T., Walsh A.G., Yu J. and Zhang P. (2021). Single-atom alloy catalysts: structural analysis, electronic properties and catalytic activities, *Chemical Society Reviews,* **50**, 569–588.

Zhu D., Chen Y. and Yang H. (2020). Synthesis and characterization of magnesium oxide nanoparticle-containing biochar composites for efficient phosphorus removal from aqueous solution, *Chemosphere*, **247**, 125847.